Numerical simulation of medium energy heavy ion reactions

J. Aichelin and G. Bertsch
University of Tennessee, Knoxville, Tennessee 37996
and Physics Division, Oak Ridge National Laboratory, Oak Ridge, Tennessee 37831
(Received 26 December 1984)

Reactions between heavy ions at medium energy are calculated using the Boltzmann-Uehling-Uhlenbeck equation. This equation incorporates the effects of a mean field as well as Pauli blocking of the nucleon-nucleon collisions. The numerical solution for two light systems, $^{16}O+^{12}C$ at 25A MeV bombarding energy and $^{12}C+^{12}C$ at 84A MeV bombarding energy, is presented and discussed in detail. In the absence of nucleon-nucleon collisions, the theory reduces to classical mean-field physics and agrees well with the quantal time-dependent Hartree-Fock theory. With collisions, the system is driven toward equilibrium even at the lower bombarding energy. The final state nucleon distribution is compared to single-particle spectra and is found to agree quite well in shape.

I. INTRODUCTION

The study of collisions between heavy ions at medium energy is a subject which is still poorly understood. At low energy, the time-dependent Hartree-Fock (TDHF) theory[1,2] provides a powerful tool for describing single-particle observables. At high energies, nucleon-nucleon collisions dominate the dynamics, and the intranuclear cascade (INC) models are applicable.[3,4] Unfortunately, the approximations in these methods are not valid in the medium energy regime. Hartree-Fock theory requires that the residual interaction be neglected in comparison to the mean field generated by the nucleons. At low energy the residual interactions have small effects because of Pauli blocking. However, at medium energy the available phase space is enlarged and the residual interactions are important, producing collisions between the nucleons.

Attempts have been made to include a collision term in TDHF calculations in order to extend the range of applicability to higher energies.[5] Due to the enormous mathematical complexity, these calculations have not yet produced useful results for interpretation of the experimental data. It should also be mentioned that the representation of quantum corrections to the mean-field theory by a collision integral may not even be well justified under the conditions found in medium-energy nucleus-nucleus collisions. In deriving a collision integral, one must assume that the time scale for the mean-field evolution is long compared with the time scale of the collisions. However, a more general approach without the collision approximation gives a theory[6] which is even more difficult to solve numerically.

Despite the theoretical uncertainties, we feel it is worthwhile to make further approximations in order to arrive at a computationally feasible theory. It appears that a manageable description from a computational point of view is obtained from a classical treatment of the single-particle density in the quantum transport equation.[7] First numerical results were obtained by the Michigan State University group.[7,8] The theory is essentially the Boltzmann equation for the single-particle distribution function, which includes both a force term, given by the gradient of the mean field, and also a collision integral of the Uehling-Uhlenbeck form.[9] The theory has the satisfying attributes of reducing to mean-field theory at low energies and to the INC model at high energies. It has been shown in one-dimensional calculations[10] that the classical mean-field theory retains most of the physics of the TDHF theory. In this work we shall extend the numerical study of the three-dimensional BUU equation to lower energies than studied in Refs. 7 and 8, and compare with TDHF as well as with some experimental single-particle spectra. The classical reduction works well for the mean-field dynamics, as we will see below.

In the next section we will review our numerical technique, which basically follows the structure of the INC method. Several modifications of the method described in Ref. 7 were necessary to apply the technique to collisions at energies below 100A MeV. Our tests to assess the validity of the numerical techniques are described in Sec. III. In Secs. IV and V we apply the theory to the reactions $^{16}O+^{12}C$ and $^{12}C+^{12}C$ at bombarding energies of 25A MeV and 84A MeV, respectively, and compare with TDHF and experimental proton spectra.

II. THEORY

For derivations of the Boltzmann-Uehling-Uhlenbeck equation (BUU) the reader is referred to Refs. 11 and 12. The equation describes time evolution of the single-particle phase space distribution function $f(p,r)$ and reads as follows:

$$\frac{\partial f_1}{\partial t}+v\cdot\nabla_r f_1-\nabla U\cdot\nabla_p f_1=-\int\frac{d^3p_2\,d^3p_{1'}\,d^3p_{2'}}{(2\pi)^9}\sigma v_{12}[f_1f_2(1-f_{1'})(1-f_{2'})-f_{1'}f_{2'}(1-f_1)(1-f_2)]$$
$$\times(2\pi)^3\delta^3(p+p_2-p_{1'}-p_{2'})\,. \tag{1}$$

Here U is the mean-field potential, which will be a specified function of the local density. With the left-hand side set to zero, the equation is the Vlasov equation, which describes the single-particle distribution evolved by a self-consistent mean field. Interpreting $f(p,r)$ as the Wigner transform of the quantum mechanical density matrix, the Vlasov equation can be derived from TDHF in the limit of smoothly varying potentials.

We need to specify both the mean-field function and the collision cross section before proceeding to the numerical details. In principle, these should be calculated by the methods of many-particle quantum mechanics, but we prefer to adopt a more heuristic approach. In the energy domain of interest, the nucleon-nucleon scattering is well described by an attractive intermediate range potential together with a hard core scattering cross section. Roughly speaking, the attractive potential gives rise to the mean field, and the hard core scattering is treated with the collision integral. We demand of the mean-field potential that it reproduce nuclear matter saturation properties and give a compressibility coefficient of $K=200$ MeV. It is not possible to achieve this with a simple functional form for the interaction; we use the following:

$$U(\rho)=-356\rho/\rho_0+303(\rho/\rho_0)^{7/6}\ (\text{MeV})\ . \tag{2}$$

As with the mean field, the collisional cross section appropriate for Eq. (1) might be quite different from the free cross section. The Pauli blocking of rescattering certainly reduces the effective cross section at low energies where the wavelength of the nucleons governs the magntiude of the coss section. Even at high energy there might be substantial differences. In one recent work,[13] for example, the collisional rate was found to be reduced by higher-order many-particle effects not included in Eq. (1) computed with free cross sections. In this work we use a constant isotropic cross section of 40 mb in Eq. (1), which we feel reasonably represents the effects of the many-particle influences.

We now outline the numerical method, which is essentially the particle-in-cell method of hydrodynamics. The phase space distribution function is represented by a collection of test particles, whose coordinates are evolved individually. For evaluation of quantities requiring the phase space density such as the potential field or the Pauli operator, the number of test particles in a cell is counted. For an accurate calculation of the potential field, the cell size should be large enough to contain many test particles. On the other hand, if the cells are too large, the nuclei would not preserve their spherical shape under the field dynamics. We found a good compromise between these conflicting demands was to take 100 test particles per nucleon and a cell size of 1 fm^3. With these numerical parameters, there are about 16 test particles in a cell at normal nuclear matter density, giving a statistical fluctuation of 25%.

Evolving the test particles by Newtonian mechanics is equivalent to solving the Vlasov equation. We use a discrete mesh in time, with a time step of 0.2 fm/c. We use first-order difference equations for the evolution of momentum and position, which actually have second-order accuracy when the momentum is evaluated at time points halfway between the times of the position determinations:

$$\mathbf{X}_n=\mathbf{P}_{n-(1/2)}\Delta t+\mathbf{X}_{n-1}\ , \tag{3}$$

$$\mathbf{p}_{n+(1/2)}=-\nabla U_n\Delta t+\mathbf{p}_{n-(1/2)}\ . \tag{4}$$

For the initial conditions we assume that the particles are distributed uniformly in spheres with a radius parameter of $r_0=1.12$ fm. The momentum distribution is given by a local Fermi gas approximation. The collision integral is treated by dividing the ensemble of test particles into individual INC simulations. Collisions are allowed between particles only in the same INC group.

The collision integral is treated in a stochastic way, allowing test particles to undergo collisions with a probability proportional to the Pauli-corrected cross section. For each time step the collisions which occur are determined as follows. The particles 1 and 2 collide in this time step if

(a) the particles pass the point of closest approach;

(b) the distance at nearest approach is smaller than $\sqrt{\pi\sigma_{\text{NN}}}$;

(c) they are not Pauli blocked.

The main numerical problem at low energies is the evaluation of the Pauli blocking factors $(1-f)$ in the collision integral. The occupation factor f is determined by examining the neighborhood of the final state phase space whenever a collision would otherwise occur. We count the number of particles in a sphere centered at the final phase space coordinates of the colliding pair. The sphere has a radius of 1 fm^{-1} in momentum space and 1.1 fm in coordinate space. The occupation factor is thus determined by

$$f(p,r)=\frac{1}{N\Omega}\sum_i^N n_i\ , \tag{5}$$

where $N=100$ is the total number of simulations, n_i is the number of particles in that volume in the ith simulation, and Ω is the phase space volume. The collision is blocked with a probability P given

$$P=1-\max[0,1-f(1)]\max[0,1-f(2)]\ . \tag{6}$$

The average number of particles in this phase space volume is around 40 for low momentum in the interior of a nucleus, so the statistical fluctuations do not cause a serious error. However, the phase space volume is too large to describe the Pauli blocking at the nuclear surface properly. In order to deal with the surface more realistically, we changed the blocking prescription in two respects. First, we divide the coordinate space sphere into halves along each coordinate plane. If the difference in the number of nucleons in pairs of half spheres exceeds the statistically expected variance, we use the more occupied of the two half spheres to determine P. Second, we distinguish projectile and target nucleons in the beginning and only allow a particle's first collision to be with a particle from the other nucleus.

III. NUMERICAL TESTS

We describe here the tests we made on the numerical method to give us confidence that we could represent the

physics of the BUU equation at energies under $100A$ MeV. One problem that immediately appears is that the longer reaction time at lower energies makes higher demands on the model to reproduce static nuclear properties. So we first examine the properties of the nuclei in their ground state by studying collisions at very large impact parameter, where nothing should change. Basically, we would like the distribution of particles in position (with respect to c.m.) and momentum to remain unchanged. One possibility to test the stability is to count the number of emitted particles. A particle is considered as emitted if first it is bound by less than 10 MeV and second, no other particle of the same simulation is closer than 2 fm. Under pure mean-field dynamics the emitted particles correspond to less than one physical particle. Allowing nucleon-nucleon collisions within each nucleus, we find that, on the average, 1.7 physical particles are emitted from the $^{16}O + {}^{12}C$ system evolved for a time of 160 fm/c. Many of these particles have scattered near the surface, where the Pauli blocker is least effective. We expect therefore that the number of artificially evaporated particles is reduced because in the actual calculations the nucleon-nucleon collisions between nucleons of the same nucleus are initially turned off. We also find that the nucleus holds its shape and rms radius very well for this time period. This tests the consistency of the assumed potential function as well as the accuracy of the numerical method.

Angular momentum conservation is important at the low energies where nuclei can stick together, but our collisional prescription does not guarantee it. However, we found that no additional effort to conserve angular momentum was required; in typical collisions the angular momentum is conserved to better than 94% on average, varying between 86% and 97%. The Pauli blocking prescription is found to be 96% effective for noncolliding nuclei. We interpret this to mean that we can apply the method to collisions in which the Pauli blocking is expected to be less than 85%; for lower energy collisions our method is not accurate enough to separate true collisions from noise. While the Pauli-blocking technique is effective in the sense of preventing nearly all collisions in a cold system, it does allow the momentum distribution to smear somewhat. However, the average kinetic energy remains close to the initial value.

IV. THE REACTION $^{16}O + {}^{12}C$ AT 25A MeV

We first study the reaction $^{16}O + {}^{12}C$ at 25A MeV bombarding energy, which has recently been studied by Gelbke *et al.*[14] The average Pauli blocking factor at 25A MeV is 0.84, to be compared with the blocking factor of 0.96 for noninteracting nuclei. Since one out of four collisions is an artifact of the numerical method, this energy is at the lower bound of applicability of our model.

For our calculations on this system, we follow the system for a time interval of 160 fm/c, examining various impact parameters. Each impact parameter calculation requires 4 h of CPU time on a VAX 780 computer. Figure 1 shows the density profiles for a range of impact parameters. The vertical frames show the system at time intervals of 20 fm/c.

We see a clear separation between three domains: a region of inelastic scattering at small and large impact parameters, separated by a fusion region at intermediate impact parameters.

The collisions at the lower impact parameter show complete momentum transfer without fusion. Much of the dissipation takes place already in the first stage of the reaction. At 20 fm/c 30% of the linear momentum is transferred, and the central density in the central region has increased to $1.3\rho_0$. At 40 fm/c 700 collisions have occurred, and the scattered particles have an increased kinetic energy (measured with respect to their local rest frame) by about 20%. This causes the system to expand in coordinate space. The density decreases to 0.80 nuclear matter density at 60 fm/c. However, the potential field at the surface is still quite attractive and most of the particles are pulled back, restoring the residues to normal nuclear matter density after 140 fm/c. After 160 fm/c the nuclei are clearly separated, having exchanged 25% of their nucleons. 77% of the nucleons remain in the residues with an excitation energy of 41 MeV. The others are free particles with a spherically symmetric momentum distribution. Thus we see a distribution of emitted particles similar to the thermal source models, although the system does not fuse. Fusion occurs for impact parameters starting with $b=2.8$ fm. Thus there is an analogy in the BUU physics to the fusion window found in TDHF calculations at low energy. Comparing with the lower impact parameter collision, there are 10% less nucleon-nucleon collisions but more interchange of nucleons in the $b=2.8$ fm collision. After 160 fm/c, projectile and target nucleons have also the same distribution in coordinate space. Although the system is not spherical at that time, one sees clearly the transition from a prolate towards a spherical shape. The system rotates, sharing some of the initial angular momentum with most of the angular momentum carried off by the emitted particles. The residue appears to have very little angular momentum, but the lack of complete angular momentum conservation in our model does not allow a small residual angular momentum to be reliably calculated. The transition from fusion to deep inelastic scattering is found at $b=4.2$ fm. Although initially the time evolution is very similar to the $b=3.8$ fm reactions, the neck between the nuclei decreases as a function of time. The system develops into two nuclei joined by a neck which are nearly at rest. If Coulomb and centrifugal forces are present, the nuclei would separate with very low kinetic energy. Finally, at an impact parameter of $b=4.9$ fm, we are in the regime of peripheral reactions. The reaction is still highly inelastic, with 50% momentum transfer, but both remnants remain spherical, have normal nuclear matter density, and emerge at a deflection angle of $-52°$.

One observable directly calculable from these runs is the fusion cross section. Since the boundaries for fusion are in between 2.2 fm $< b \leq 2.8$ fm and 3.8 fm $< b < 4.2$ fm, the predicted fusion cross section is in between 200 and 400 mb.

It is of interest to compare the classical collisionless

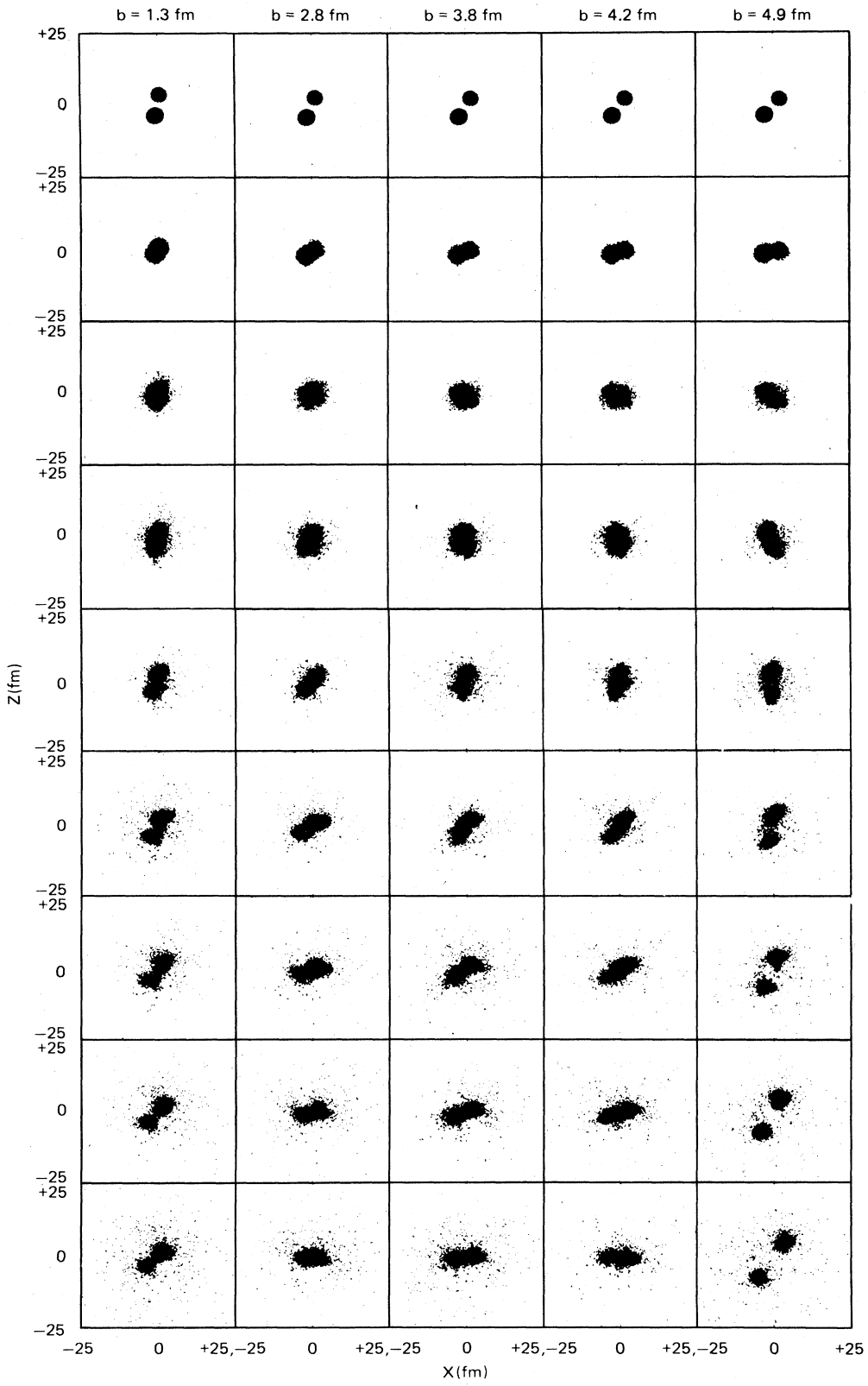

FIG. 1. Overview of the numerical simulation of the reaction $^{16}O + ^{12}C$ at 25A MeV bombarding energy. The coordinates of all 2800 particles are projected onto the xy plane, where z is the beam axis and x the direction of the impact parameter. For five impact parameters (b=1.3, 2.8, 3.8, 4.2, and 4.9 fm) the reaction is displayed in time intervals of 20 fm/c.

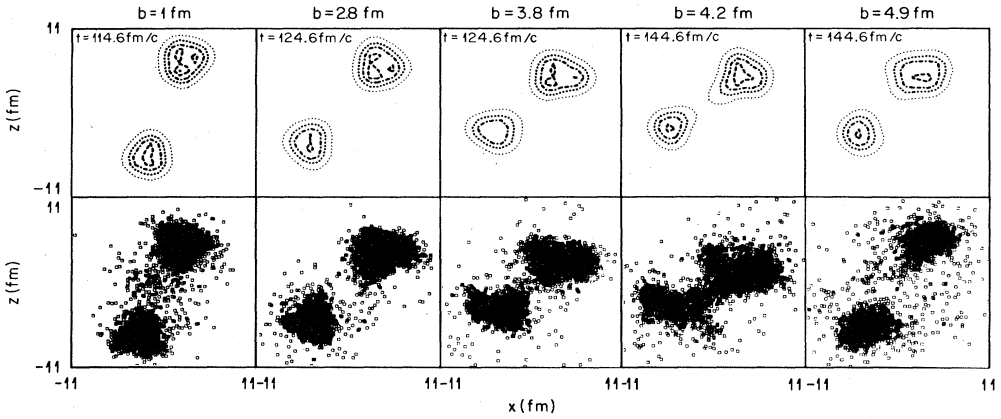

FIG. 2. Density projection of the $^{16}O + ^{12}C$ system, comparing the mean field theory Eq. (3a) with THDF results. For five different impact parameters ($b = 1.3$, 2.8, 3.8, 4.2, and 4.9 fm) the final results of both calculations are displayed.

dynamics with TDHF theory, which does the same physics quantum mechanically. In Fig. 2 we show the Vlasov results at varying impact parameters compared with TDHF results provided by Stoecker and Cusson.[15] Fusion is absent in both theories and the predictions of energy loss and deflection angles are quite similar. Thus the conclusions of comparisons between quantum and classical mean-field theories in one dimension[10] extend to realistic three-dimensional calculations as well.

Another simple experimental observable is the single-particle spectra of particles emitted from the reaction system. In many circumstances the single-particle spectra can be described by a thermal source, which assumes that the energy and the momentum are shared statistically among a group of nucleons. The angular distribution is then isotropic in the frame of the source and the energy spectrum is exponential with a characteristic temperature determined from energy conservation. We will now examine how well these features show up in our model. Figure 3 compares the theoretical proton spectra (in the lab) compared to measurements of Gelbke.[14] We see that the slope agrees well with the data at all angles except for the most forward. The fact that the theoretical distributions approach exponential shows that not many collisions are necessary to thermalize the system, as far as can be determined from the single-particle spectra. The magnitude of

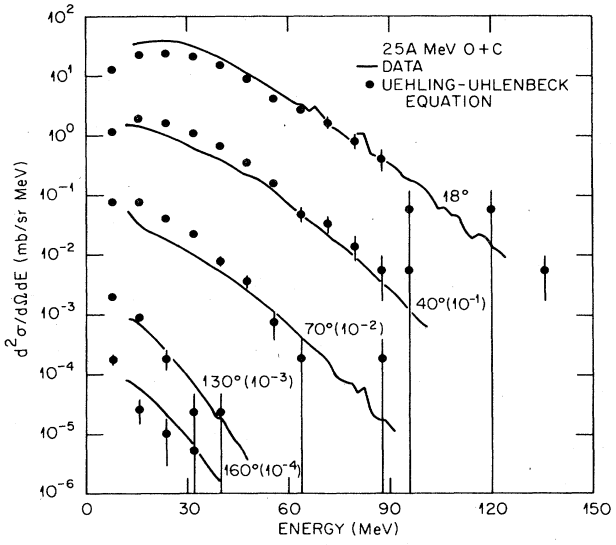

FIG. 3. The proton spectra in the reaction $^{16}O + ^{12}C$ at 25A MeV, comparing theory with experimental data of Gelbke *et al.* (Ref. 14). The curves show the energy spectra at angles of 18°, 40°, 70°, 130°, and 160° with curves displayed by a factor of 10 for clarity in the figure.

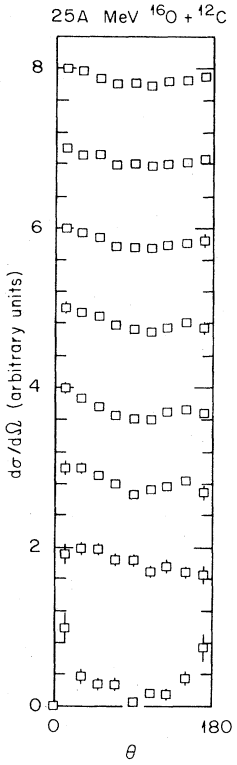

FIG. 4. Angular distribution of the emitted particles as a function of time in steps of 20 fm/c. The particles emitted in the first time interval are shown on the bottom curve and the higher curves show the accumulated particle distribution at successive steps of time.

TABLE I. Final kinetic energy of the fragments and deflection angle for TDHF, Vlasov, and BUU equations for five impact parameters ($b=1.3$, 2.8, 3.8, 4.2, and 4.9 fm) for the reaction 25A MeV $^{16}O + {}^{12}C$.

Impact parameter (fm)		1.3	2.8	3.8	4.2	4.9
THDF	E frag (MeV)	75	67	47	29	39
	theta	−28°	−58°	−80°	−90°	−91°
Vlassov	E frag (MeV)	37	55	32	26	50
	theta	−43°	−68°	−84°	−111°	−66°
BUU	E frag (MeV)			at rest		44
	theta					−52°

the theoretical cross section is systematically too high except at the most forward angle at low energies. This discrepancy is undoubtedly due to the inadequate treatment of clusters in mean-field theory. The theory predicts that essentially all emitted particles are free, but experimentally many particles form clusters on their way out. Thus the experimentally measured proton cross section is reduced. At low energy and the most forward angles the theory has the opposite tendency, underpredicting the cross section. This is probably due to the emission of nucleons in the final state from the excited nuclei in the exit channel. We find that the average excitation energy in the system at 160 fm/c is 40 MeV, so several nucleons could easily be emitted.

The angular distribution of emitted particles in the c.m. system is shown as a function of time in Fig. 4. At early times, shown in the bottom of the figure, the distribution is peaked along the beam axis. The distribution becomes nearly isotropic for particles emitted at later times. Also, the out-of-plane correlation is moderate; we find $\sigma(\phi=90°)/\sigma(\phi=0°)=0.73$. As would be expected with a system evolving toward equilibrium, the earliest particles are most energetic on the average. The later isotropic component has a lower energy, consistent with the thermal source estimates.

The question of whether the thermal source is spatially localized in the geometric overlap region between the two nuclei has caused much discussion.[16–18] In this picture the nucleons in the overlap region between target and projectile form a highly excited subsystem. In our calculation we find that the emitted particles arise from other regions of the nuclei as well as from the overlap region. This shows that the system considered is too small, in relation to the interaction range, to show a geometrically localized hot spot.

The dependence of multiplicity on impact parameter has been a useful quantity for interpreting collision at higher energies, so we examined this dependence at 25A MeV in our model. We find there is no strong dependence on impact parameter. The charge multiplicity varies from $\langle Z \rangle = 3.2$ for head-on collisions to 2.5 for peripheral collisions at $b=5.2$ fm. However, it should be mentioned that after 160 fm/c, the reaction products still have a substantial excitation energy which will give rise to further evaporation.

Finally, we examine the energy loss and the deflection of fragments in the final state. As mentioned earlier, the BUU equation predicts complete momentum transfer up to impact parameters of 3.8—4.2 fm. Above that, there is nuclear scattering with large energy loss and deflection angle. We display these quantities in Table I. However, as may be seen from Table I, also in the mean-field theories the nuclei lose a considerable amount of their initial energy.

V. THE REACTION $^{12}C + {}^{12}C$ AT 84 A MeV

Collisions of $^{12}C + {}^{12}C$ at 84A MeV have been studied in several experiments at CERN.[19–21] The BUU model of the dynamics should be more reliable at this higher energy, because the Pauli blocking is less critical, and also because the greater phase space available will make the collision approximation more accurate. As for the previous system, we will examine the density profile as a function of time and impact parameters and calculated the single-particle observables predicted by the model. Figure 5 shows the density profiles for the two impact parameters, $b=1$ and 2.8 fm, plotted at 20 fm/c time intervals.

At the lower impact parameter there are many nucleon-nucleon collisions in the early stage of the reaction. By 20 fm/c 900 collisions have already occurred, despite 60% blocking due to the Pauli principle. The systems becomes quite spherical, and more than 50% of the momentum is transferred. The kinetic energy of scattered particles is twice as large in the c.m. frame compared to that of those which have not scattered. The central density is normal nuclear matter density at 20 fm/c, but the system continues to expand as time goes on. By 120 fm/c the system has disassembled and dispersed. On the average, 14.5 particles are evaporated. Although there appears to be concentration of particles in the figure, in fact the density never exceeds $\frac{1}{2}$ of nuclear matter density. In all likelihood, there would be much clustering in the final state, but that is not calculable in our model. There is a transition at $b=2$ fm from a spherical disassembly to a peripheral reaction with participant-spectator characteristics, without a region of deep inelastic scattering in between. In other words, the nuclei have too much energy to be simply slowed down without becoming completely destroyed. An example of peripheral reactions is shown for $b=2.8$ fm. One sees a behavior similar to that found in high energy reactions: There is a separation between targetlike and projectilelike fragments and an overlap region that is a source of particle emission. At 20 fm/c, some fast particles have already emerged in forward-backward directions. By 60 fm/c the spectator remnants are already well separated, and have normal density by 80

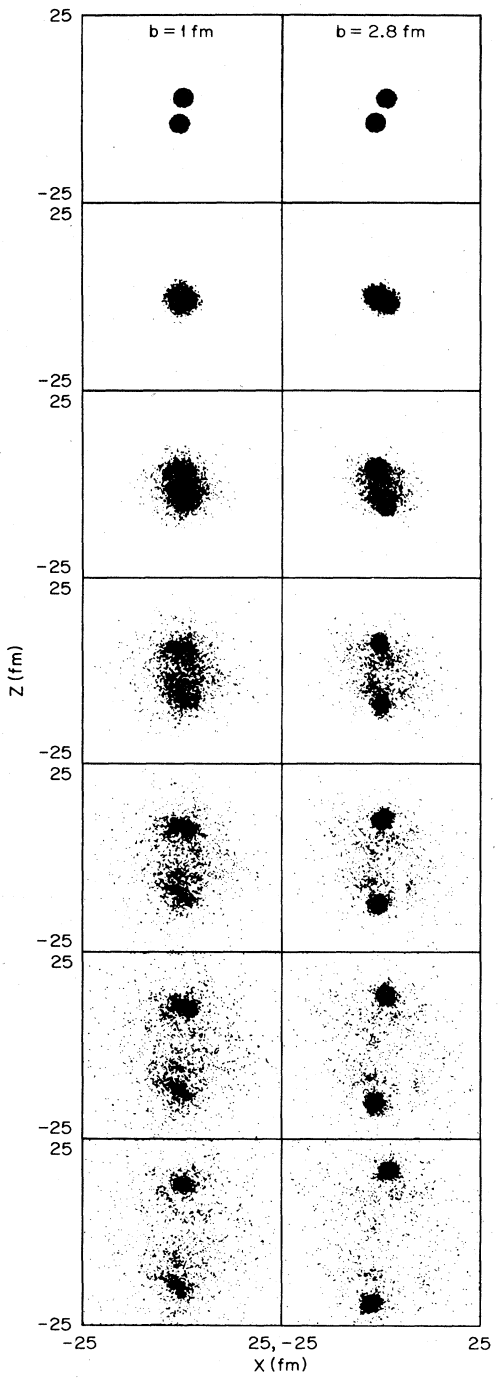

FIG. 5. Overview of the numerical simulation of the reaction $^{12}C + ^{12}C$ at 84A MeV bombarding energy. The coordinates of all 2400 particles are projected onto the xy plane, where z is the beam axis and x the direction of the impact parameter. For two impact parameters ($b=1$ and 2.8 fm) the reaction is displayed in time intervals of 20 fm/c.

fm/c. Dividing the particles according to the region of origin the overlap region is 22% more likely to emit particles than the spectator zones. The particles from the overlap region have also suffered a significantly higher number of collisions (1.5 compared to 1.2) and therefore

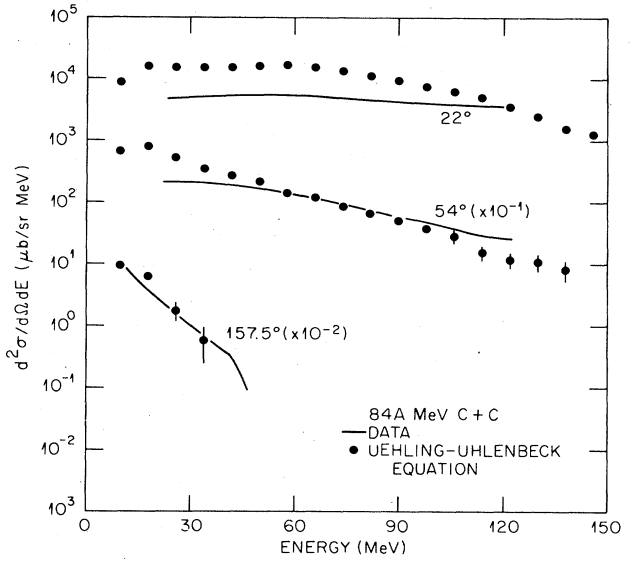

FIG. 6. The proton spectrum in the reaction $^{12}C + ^{12}C$ at 84A MeV, comparing theory with the data of Santo *et al.* (Ref. 19). The curve shows the energy spectrum at angles of 22°, 54°, and 157.5°.

have a more thermal spectrum. This is obviously the medium energy equivalent of a fireball. In the final state at $b=2.8$ fm the energy is distributed as follows: 36% in the relative motion, 53% in evaporated particles, and the rest in the excitation energy of the remnants.

Proton spectra of the reaction are measured in Refs. 19—21, and we compare our calculation with these data. The energy distributions at the three measured angles of Ref. 19 are shown in Fig. 6. The measurements of Refs. 20 and 21 are shown in Fig. 7. As found earlier, the relative ratio and the slope agree well for the larger angles but not for the most forward angle. We agree better in shape

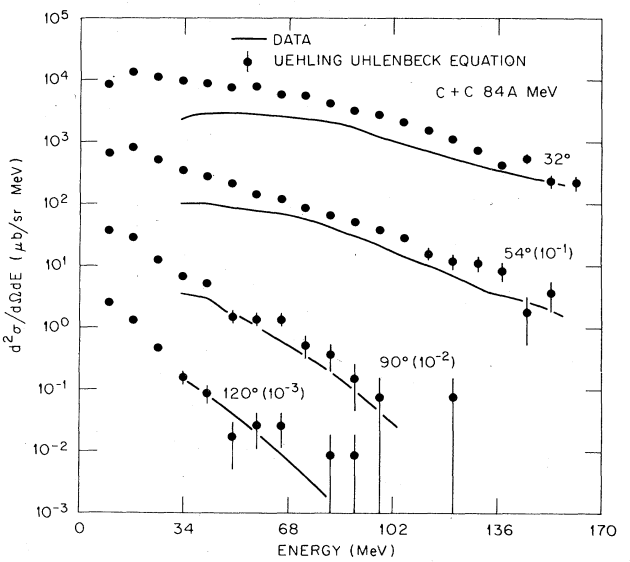

FIG. 7. The proton spectrum in the reaction $^{12}C + ^{12}C$ at 84A MeV, comparing theory with the data of Refs. 20 and 21. The curve shows the energy spectrum at angles of 32°, 54°, 90°, and 120°.

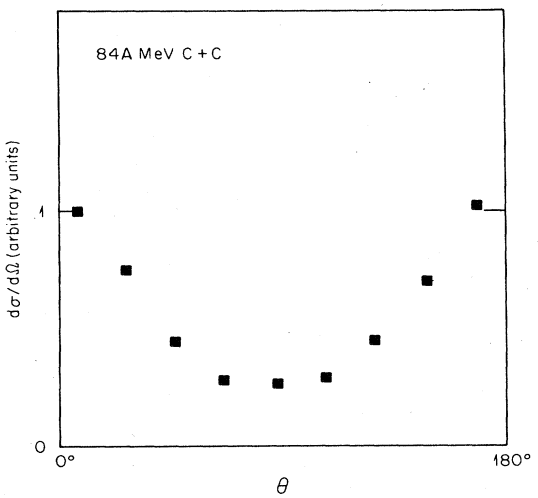

FIG. 8. Angular distribution of emitted particles in the reaction $^{12}C + ^{12}C$ at 844 MeV. The curve shows the calculated center-of-mass angular distribution of emitted particles at 120 fm/c.

with the data of Jakobsson *et al.*[19,20] at four angles they measured between 32° and 120°. However, the overall normalization of that data is 1.5 lower than those of Ref. 19, and so our calculation overpredicts the data. As mentioned earlier, the theory does not properly treat clustering, and therefore we expect a larger cross section. To address the question of equilibrium emission, we shown in Fig. 8 the angular distribution of the emitted particles in the c.m. frame. The particles around 90 deg arise mainly from small impact parameters and have suffered on the average more collisions than those contributing to the forward/backward spectra, which also have a higher average kinetic energy. Also here we do not find a strong dependence on the out-of-plane angle. The ratio of emission probability at $\phi = 90°$ to $\phi = 0°$ is 0.84.

The ratio of the final to the initial momentum *Pz* associated with one of the reaction partners is displayed in Fig. 9. For central collisions 75% of the momentum is

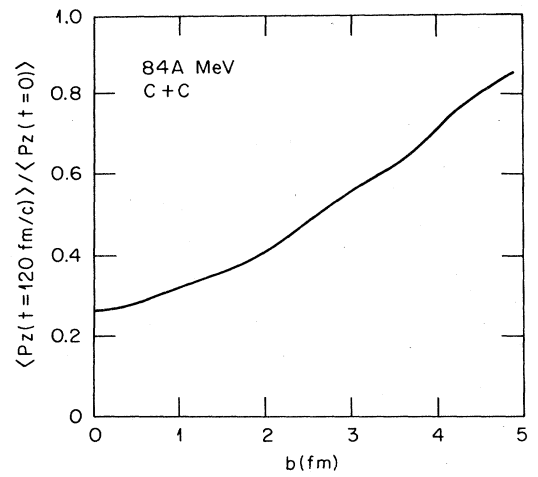

FIG. 9. The graph shows the ratio of the final to initial momentum p_z associated with particles of one of the reaction partners.

transferred. Hence ^{12}C nuclei at 844 MeV are not able to completely stop each other. In contrast to the 254 MeV $^{16}O + ^{12}C$ reaction, the 844 MeV $^{12}C + ^{12}C$ system shows a strong impact parameter dependence of the multiplicity of the evaporated particles. It varies from 14.5 at $b=1$ fm to 3.6 at $b=4.9$ fm.

VI. CONCLUSIONS

Our study of the classical mean-field theory with the Uehling-Uhlenbeck collision integral shows two general features that make the theory appear to be very useful for analyzing single-particle observables in medium-energy heavy-ion collisions. First, we found that the collisionless mean-field theory reproduced the results of TDHF quite well at 254 MeV, and the agreement is even better at 844 MeV.

This confirms and extends comparisons made in one dimension,[10] and shows that the quantum physics is not really important for the mean-field behavior, once the initial single-particle distribution is properly specified. At 254 MeV, the Uehling-Uhlenbeck equation predicts fusion for intermediate impact parameter reactions, whereas in mean-field theory there is complete transparency for all impact parameters at this energy. The single-particle spectra show two components: an early preequilibrium component which is strongly peaked in forward-backward direction from the first particles emitted and a nearly isotropic thermal component of the later particles, which gives most of the cross section at 254 MeV. The energy distribution of the particles approximates an exponential, which, however, varies in slope depending on the angle in the center of mass. Thus the theory predicts definite differences from the thermal source models that postulate complete equilibrium. At higher energies the nuclei cannot transfer enough momentum to fuse, but there is still a very large linear momentum transfer and kinetic energy loss of the final state nuclei. So far this domain has not been studied very well experimentally; measurements of linear momentum transfer on heavy targets show that linear momentum transfer is complete at low energies and falls off smoothly to energies of the order to 100A MeV.[22]

There is also a large momentum loss in the mean-field theory, but it is not nearly as complete as we find it with the BUU equation. The basis question is the degree of equilibration in collisions at these intermediate energies, and while our method appears to be a useful tool for studying this question, some cautions should be noted. The intrinsic and numerical approximations in our description could bias the conclusions in either direction. The actual quantum physics might be more dissipative because the many-particle wave function has correlations already in the initial state which are neglected in the BUU equation. Expressed in different language, the off-shell propagation of particles could lead to additional energy loss mechanisms not calculated in our on-shell theory. On the other hand, the classical BUU equation is likely to overestimate the dissipation as compared with the extended TDHF calculations because the continuum approximation to phase space in classical physics allows transitions that would be quantum mechanically forbidden. Finally, on a purely numerical level, the Pauli blocking technique

is less than perfect. We feel it is adequate but have no way of checking beyond examining the fraction of collisions blocked. We are currently extending the calculation to larger target masses, where the distinction between the emission source and the spectator matter should be clearer. Also much more detailed data are available for larger targets.

ACKNOWLEDGMENTS

This research was sponsored by the National Science Foundation under Grant PHY-84-13287 and by the Division of Nuclear Physics, U.S. Department of Energy under contract DE-AC05-840R21400 with Martin Marietta Energy Systems, Inc.

[1]K. T. R. Davies, K. R. S. Devi, S. E. Koonin, and M. R. Strayer, in *Heavy-Ion Science,* edited by D. A. Bromley (Plenum, New York, 1984).
[2]J. Negele, Rev. Mod. Phys. **54**, 913 (1982).
[3]J. Cugnon, Phys. Rev. C **22**, 1885 (1980).
[4]Y. Yariv and Z. Fraenkel, Phys. Rev. C **29**, 2227 (1979).
[5]C. Y. Wong and K. T. R. Davies, Phys. Rev. C **28**, 240 (1983).
[6]B. Buck and H. Feldmeier, Phys. Lett. **129B**, 223 (1983).
[7]G. Bertsch, H. Kruse, and S. Das Gupta, Phys. Rev. C **29**, 673 (1984).
[8]H. Kruse, B. Jacak, and H. Stoecker, Phys. Rev. Lett. **54**, 289 (1985).
[9]E. Uehling and G. Uhlenbeck, Phys. Rev. **43**, 552 (1933).
[10]H. Tang *et al.*, Phys. Lett. **101B**, 10 (1981).
[11]L. P. Kandanoff and G. Baym, *Quantum Statistical Mechanics* (Benjamin, New York, 1962).
[12]H. Mori, Prog. Theor. Phys. **8**, 327 (1952).
[13]P. Danielewicz, Ann. Phys. (N.Y.) **152**, 305 (1984).
[14]C.-K. Gelbke, private communication.
[15]R. Cusson and H. Stoecker, private communication.
[16]W. A. Friedman and W. G. Lynch, Phys. Rev. C **28**, 16 (1983).
[17]J. Aichelin, J. Huefner, and R. Ibarra, Phys. Rev. C **30**, 107 (1984).
[18]J. Aichelin, Phys. Rev. Lett. **52**, 2343 (1984).
[19]R. Santo, private communication.
[20]A. Oskarsson, Lund University Report 8303, 1983.
[21]B. Jakobsson *et al.*, Phys. Lett. **102B**, 121 (1981).
[22]G. La Rama *et al.*, Nucl. Phys. **A407**, 233 (1983).